IEEE Access
Multidisciplinary ⋮ Rapid Review ⋮ Open Access Journal

Received 2 December 2023, accepted 10 January 2024, date of publication 19 March 2024, date of current version 28 March 2024.

Digital Object Identifier 10.1109/ACCESS.2024.3378737

RESEARCH ARTICLE

DSSCNet: Deep Custom Spatial and Spectral Consistency Layer-Based Dehazing Network

MANJIT KAUR[1], (Senior Member, IEEE), DILBAG SINGH[2,3,4], (Senior Member, IEEE), VIJAY KUMAR[5], (Member, IEEE), UMASHANKAR RAWAT[6], (Member, IEEE), AND MOHAMMED AMOON[7]

[1]School of Computer Science and Artificial Intelligence, SR University, Warangal, Telangana 506371, India
[2]Department of Radiology, Center of Biomedical Imaging, New York University Grossman School of Medicine, New York, NY 10016, USA
[3]Research and Development Cell, Lovely Professional University, Phagwara, Punjab 144411, India
[4]Centre of Research Impact and Outcome, Chitkara University Institute of Engineering and Technology, Chitkara University, Rajpura, Punjab 140401, India
[5]Department of Information Technology, Dr. B. R. Ambedkar National Institute of Technology, Jalandhar, Punjab 144008, India
[6]Department of Computer Science and Engineering, School of Computer Science and Engineering, Manipal University Jaipur, Jaipur 303007, India
[7]Department of Computer Science, Community College, King Saud University, Riyadh 11437, Saudi Arabia

Corresponding authors: Manjit Kaur (manjit.kaur@sru.edu.in) and Umashankar Rawat (umashankar.rawat@jaipur.manipal.edu)

This work was supported by the Researchers Supporting Project number (RSPD2024R968), King Saud University Riyadh, Saudi Arabia.

ABSTRACT Poor weather conditions, such as haze, fog, and smog, present significant challenges in capturing clear and visually appealing images. Though the existing image dehazing algorithms have achieved significant performance, they still suffer from various problems such as generalization to diverse hazy conditions, potential artifact generation, and computational complexity. Additionally, sensitivity to parameter settings, haze density variability, image content, noise, and scene-specific information remains areas of concern. To address these issues, we propose a Deep Custom Spatial and Spectral Consistency Layer-based Dehazing Network (DSSCNet) that effectively removes haze from images while preserving important spatial and spectral details. The network architecture includes a custom Haze Removal Layer (HRL), convolutional layers with ReLU activation, pooling layers, skip connections, and a custom Spatial and Spectral Consistency Layer (cSSCL). HRL estimates atmospheric light and transmission maps to generate an intermediate haze-free image. The proposed loss function combines Mean Squared Error (MSE) loss with a Consistency Loss (CL) to encourage content preservation during dehazing. Extensive experimental results demonstrate that DSSCNet outperforms competitive models in terms of various performance metrics, including contrast gain (c_g), new visible edges (e), new edge gradients ($\bar{r}$), Peak Signal-to-Noise Ratio (PSNR), and Structural Similarity Index (SSIM) by average improvements of approximately 1.27%, 1.12%, 1.18%, 1.21%, and 1.24%, respectively.

INDEX TERMS Dehazing, deep learning, convolutional neural network, atmospheric light, transmission map, spatial and spectral consistency, haze removal, image enhancement, image dehazing, optimization, Adam optimizer.

I. INTRODUCTION

Image dehazing is a crucial image processing task that aims to improve visibility and restore clear details in images that are affected by atmospheric haze, fog, or other adverse environmental conditions [1], [2]. Haze in images causes a reduction in contrast, color saturation, and sharpness, making it challenging for humans and computer vision systems to perceive and analyze visual content accurately [3], [4]. Dehazing techniques play a vital role in various real-world applications, including surveillance, autonomous vehicles, remote sensing, and outdoor photography, where visibility is often compromised due to weather conditions or pollution [5]. The physical process of haze formation occurs

The associate editor coordinating the review of this manuscript and approving it for publication was Wenming Cao.

due to the scattering and absorption of light by particles and molecules present in the atmosphere [6]. Light from objects in the scene interacts with these particles, leading to multiple scattering events. These events result in the loss of image details and degradation of visual quality. Traditional image dehazing methods often model the atmospheric scattering process and aim to estimate and remove the haze from the observed images [7]. These approaches typically rely on various image priors, hand-crafted features, or physical constraints to achieve dehazing.

A. BACKGROUND

In recent years, data-driven approaches based on deep learning have gained immense popularity in the field of image dehazing [8]. Convolutional Neural Networks (CNNs) have shown exceptional performance in various computer vision tasks, including dehazing, defogging, desmogging, etc. Deep learning-based dehazing methods learn complex mappings between hazy and clean image pairs from large-scale datasets, enabling them to generalize well to different haze conditions and improve dehazing quality [8]. These techniques have demonstrated superior performance compared to traditional methods, as they can capture intricate image features and implicitly learn the complex scattering and absorption phenomena. One of the key advantages of deep learning-based dehazing is its ability to generalize well to real-world scenarios, including those with non-uniform haze distributions, varying scene complexities, and diverse lighting conditions [9]. These methods can effectively restore details in challenging scenarios, such as underwater and nighttime dehazing, where traditional approaches often struggle to provide satisfactory results [10].

Moreover, researchers have explored innovative approaches that integrate domain-specific information, such as polarization information in underwater dehazing, to further enhance the dehazing process [10]. These techniques leverage the physical properties of light polarization to better estimate and remove the scattered light from underwater scenes, resulting in improved visibility and image quality. As image dehazing continues to be a subject of extensive research, the field is witnessing ongoing advancements in model architectures, loss functions, and data augmentation techniques. Real-time dehazing methods are being developed to meet the needs of applications with strict latency requirements, such as real-time video processing for autonomous vehicles and surveillance systems [11]. In this ever-evolving landscape of image dehazing, researchers work to tackle the challenges posed by various environmental conditions and achieve natural, artifact-free, and visually pleasing dehazed images [8]. The integration of physical models, deep learning, and domain-specific information shows great promise in advancing the capabilities of image dehazing, facilitating practical and effective solutions across a broad spectrum of real-world applications [9].

Recently, researchers have proposed various deep learning architectures for image dehazing. These advancements aim to improve image quality and visibility in various hazy conditions for different applications, including remote sensing, high-resolution dehazing, and multi-agent reinforcement learning [12]. Methods like Hadamard-Product (HP) models [13] and deep dehazing networks achieved realistic dehazing and handled low-light and underwater scenarios [13], [14]. Transfer learning and feedback mechanisms were used to enhance dehazing performance [15], [16], while unsupervised methods relied on deep image prior [17]. Over time, researchers have developed various dehazing techniques, which can be categorized as prior-based methods, deep learning approaches, and fusion strategies.

1) PRIOR-BASED APPROACHES

The foundation of image dehazing lies in prior-based methods such as the dark channel prior (DCP) [18], [19] and atmospheric scattering models [20]. These methods involve estimating critical parameters like transmission maps and atmospheric light to remove haze from images. However, these methods often rely on simplified atmospheric models that may not fully capture the complexities of real-world scenarios. Although effective, their assumptions can limit their performance in challenging environments.

2) DEEP LEARNING REVOLUTION

The emergence of deep learning, particularly convolutional neural networks (CNNs), has revolutionized the field of image dehazing. Techniques like Light-DehazeNet [21] and cascaded CNNs [22] harness the power of deep networks to jointly estimate transmission maps and atmospheric light, resulting in substantial improvements in dehazing performance. The integration of adversarial learning strategies [14], [23] further enhances the restored images, achieving more natural dehazing results.

3) FUSION-BASED STRATEGIES

Fusion-based methods, such as the Fusion-Based Variational Image Dehazing (FVID) approach [24], utilize optimization frameworks to combine the outcomes of different dehazing models. This fusion strategy tackles challenges related to contrast, saturation, and image structure preservation, leading to enhanced dehazing outcomes. By integrating distinct sources of information, these methods effectively reduce the impact of haze, thereby enhancing image clarity.

4) CHALLENGES AND SPECIALIZATION

Addressing specific challenges, like nighttime dehazing, has spurred the development of specialized methods [25], [26]. These methods take into account the unique characteristics of low-light conditions and adaptively estimate atmospheric light. As a result, they effectively enhance visibility and mitigate artifacts associated with nighttime imaging. Furthermore, techniques such as linear transformations [27] present efficient alternatives for image dehazing.

B. MOTIVATION AND CONTRIBUTIONS

Existing image dehazing algorithms have made significant progress, but they still face limitations such as challenges in generalization to diverse hazy conditions, potential artifact generation, and computational complexity. Additionally, sensitivity to parameter settings, haze density variability, image content, noise, and scene-specific information remains areas of concern. Overcoming these limitations is crucial for advancing image dehazing techniques to achieve more robust and reliable results in various real-world scenarios.

To overcome these limitations, this paper makes the following contributions:

1) To effectively remove haze while preserving important image details, including spectral and spatial information, two custom layers are designed: the Haze Removal Layer (HRL) and the Spatial and Spectral Consistency Layer (cSSCL).
2) To improve information flow and feature extraction, skip connections are used.
3) A consistency term is added to the loss function to encourage the preservation of spatial and spectral information of the images during the dehazing process.

Remainder of the paper is structured as follows: Section II provides an overview of the related work. In Section III, the proposed Deep cSSCL-based Dehazing Network (DSSCNet) is discussed. The comparative analysis of DSSCNet is presented in Section IV. Finally, Section V concludes the paper.

II. RELATED WORK

Kalra et al. proposed a novel deep learning architecture for dehazing of aerial remote sensing images [28]. The authors introduced an end-to-end deep learning network (EEDNet) that efficiently restored aerial remote sensing images by directly computing the relationship between hazy and clear images. This architecture eliminated many assumptions made in other models and achieved realistic dehazed images by identifying structural and statistical portions separately from the image. Han et al. proposed DeHRNet, a high-resolution network for single image dehazing [29]. DeHRNet utilized a modified network originally designed for human pose estimation. The authors introduced a new stage that enhanced high-resolution representations, leading to superior dehazing performance over existing methods in synthesized and natural hazy images. Wu et al. introduced a three subnets dehazing network (TSDNet) based on transfer learning [15]. The authors presented a CNN with transfer learning that improved dehazing performance, particularly in nonhomogeneous hazy map datasets. Their approach enhanced model efficiency, haze removal quality, and generalization ability in small-scale datasets.

Yu et al. utilized deep reinforcement learning for aerial image dehazing [30]. The authors proposed DRL_Dehaze, a multi-agent deep reinforcement learning network, which automatically selected the most suitable dehazing method in multi-scale haze situations, achieving good dehazing results on various ground types. Song et al. explored the use of vision transformers for single image dehazing and introduced DehazeFormer, an improved Transformer architecture [12]. DehazeFormer outperformed existing methods on image dehazing datasets and achieved state-of-the-art results, demonstrating the potential of Vision Transformers in the field of image dehazing. Liu et al. proposed a Hadamard-Product (HP) model for image dehazing, consisting of data-driven priors and a Learnable Hadamard-Product-Propagation (LHPP) approach [13]. The LHPP used principle-inspired guidance and recovery modules to eliminate noises/artifacts during the dehazing process, leading to more realistic outputs. HP model was also extended to solve low-light image enhancement and underwater image enhancement problems.

Li et al. proposed a deep dehazing network (DDNet) with latent ensembling architecture and adversarial learning [14]. The network addressed issues with inaccurate estimation of transmission and atmospheric light in hazy images by using a multi-task generator and a multi-scale discriminator. The approach achieved end-to-end photo-realistic dehazing, with superior performance over other methods in various benchmarks. Song and Liu introduced CPAD-Net, an improved dehazing network with attention mechanisms and dense residual blocks [31]. The network effectively captured non-uniform haze distribution and reconstructed clearer dehazed images with improved texture detail information and color recovery. Comparative evaluations demonstrated the superiority of CPAD-Net against other dehazing algorithms. Liang et al. proposed a Progressive Single-Image Dehazing Network with Feedback Mechanism (PFBN) [16]. PFBN used a recurrent structure with feedback blocks to improve the dehazing process and preserve ground information. An enhancement self-ensemble strategy further enhanced the dehazing results, and extensive experiments validated the effectiveness of PFBN.

Xu and Wei presented an unsupervised single-image dehazing method called "Pyramid Deep dehazing (PDL)" that utilized deep image prior [17]. The method was based on the optical model of haze and other haze-like degradation images. The Pyramid deep image strategy gradually generated clear background without the need for extra data or handcrafted priors, making it effective for various haze-like degradation scenarios. Parihar and Gupta developed a neural network for image dehazing based on two phases: estimating the transmission map and performing haze removal [32]. The network avoided estimating ambient light and achieved improved dehazing performance.

However, the existing image dehazing techniques exhibit several limitations. Most of the existing approaches relying on handcrafted priors often struggle to accurately estimate the complex characteristics of real-world hazy images, leading to suboptimal results in challenging scenarios [3]. Moreover, many deep learning-based methods heavily depend on training data, making them less adaptable to different datasets and hazy conditions [13]. Inaccurate estimation

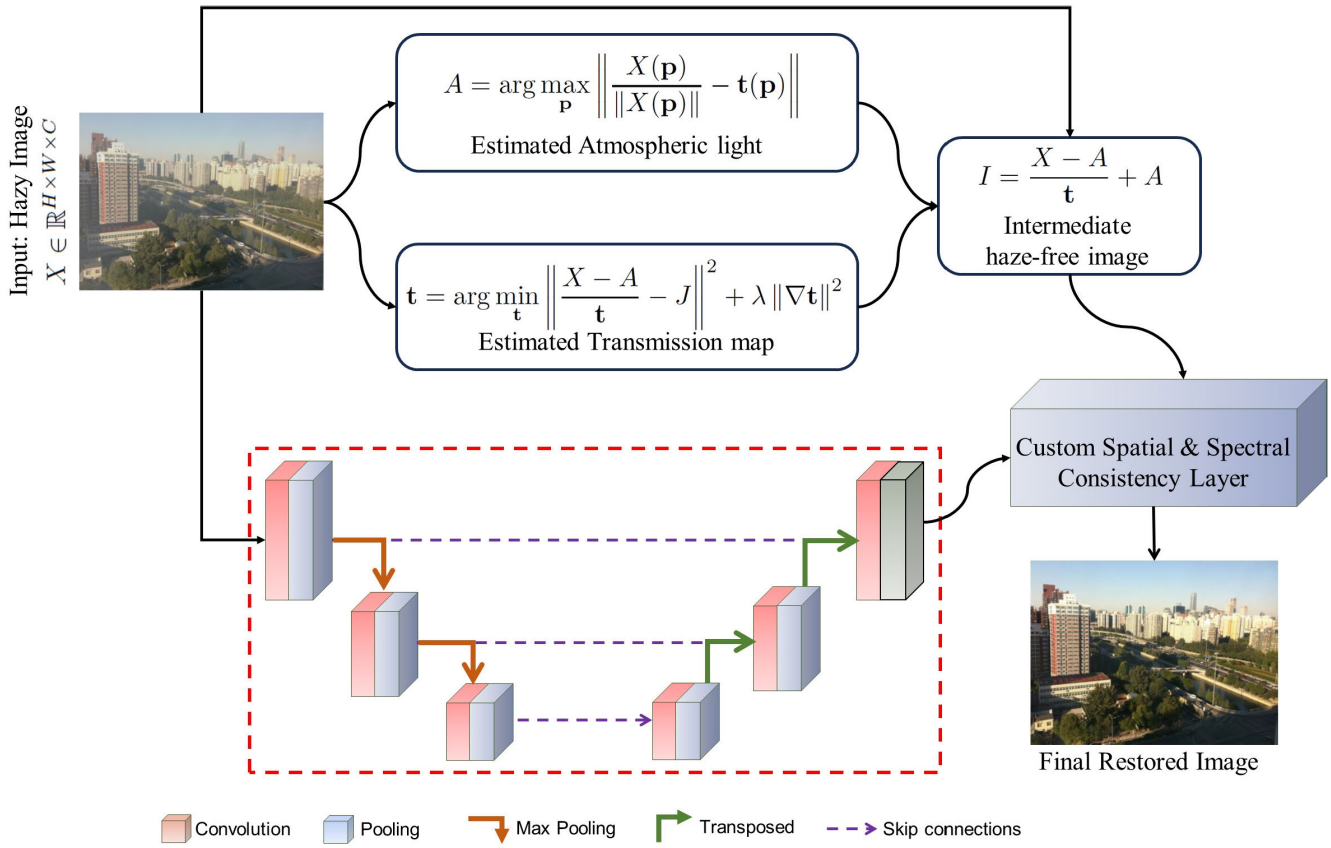

FIGURE 1. Diagrammatic flow of the proposed deep custom spatial and spectral consistency layer-based dehazing network.

of transmission and atmospheric light in hazy images can further compromise the realism of dehazed outputs [14]. Additionally, certain techniques may encounter difficulties in handling non-uniform haze distributions, resulting in inadequate haze removal from specific regions of the image [31]. The domain shift between training and testing data can affect the performance of deep learning-based methods, making them less reliable in practical applications [5]. Furthermore, preprocessing with dehazing may not always substantially improve the performance of high-level vision tasks, leading to unpredictable outcomes [5]. Some dehazing algorithms may inadvertently introduce artifacts or noises during the restoration process [13]. Limited by small-scale datasets, certain models may lack the necessary generalization ability and efficiency to handle a wide range of hazy scenarios [15]. Finally, the lack of robustness in some dehazing methods may pose challenges in achieving consistently effective results in real-world complex settings [3].

III. DEEP CUSTOM SPATIAL AND SPECTRAL CONSISTENCY LAYER-BASED DEHAZING NETWORK

A Deep Custom Spatial and Spectral Consistency Layer-based Dehazing Network (DSSCNet) is designed to effectively remove haze from hazy images while preserving spatial and spectral information. Figure 1 shows the diagrammatic flow of the DSSCNet. The architecture consists of a custom HRL, convolutional layers with ReLU activation, pooling layers, skip connections, and a custom cSSCL. HRL estimates the atmospheric light and transmission map to generate an intermediate haze-free image. Consistency Loss (CL) term is added to MSE Loss function to enforce spatial and spectral preservation during the dehazing process. The network is trained using Adam optimizer to optimize the proposed loss function.

A. ARCHITECTURE

The deep dehazing network is designed to remove haze from input images effectively while preserving spatial and spectral information. The network consists of multiple layers, including custom layers specifically designed to address haze-related challenges (refer Algorithm 1). The remaining section discusses the complete architecture.

1) INPUT LAYER

The input layer takes the hazy image $X \in \mathbb{R}^{H \times W \times C}$ as input, where H, W, and C represent the height, width, and number of channels of the input image, respectively.

2) CUSTOM LAYER 1: HAZE REMOVAL LAYER

HRL plays a crucial role in estimating and removing the haze from the input image. It aims to generate an intermediate

Algorithm 1 Proposed DSSCNet Architecture

Require: Hazy image $X \in \mathbb{R}^{H\times W\times C}$
Ensure: Dehazed output $\hat{Y}$
1: **Compute estimated atmospheric light** A using Eq. (1)
2: **Compute estimated transmission map t** using Eq. (2)
3: **Compute intermediate haze-free image** I using Eq. (3)
4: **for** $i = 1$ **to** L **do**
5: $\quad Z_i \leftarrow \text{Conv}(Z_{i-1}) + \text{ReLU}(Z_{i-1})$
6: **end for**
7: **Apply pooling layers and skip connections** to enhance feature extraction
8: **Generate dehazed output** $\hat{Y}$ using cSSCL with perceptual loss or adversarial loss
9: **Compute MSE Loss** as in Eq. (4)
10: **Compute CL** as in Eq. (5)
11: **Compute Revised Loss (RL)** as in Eq. (6) with λ as a trade-off parameter
12: **Use Adam optimizer with Algorithm 2 to optimize parameters**
13: **return** $\hat{Y}$

haze-free image I by estimating the atmospheric light and transmission map from the hazy input image X. The process of haze removal involves three main steps: estimating the atmospheric light, the transmission map, and restoration model.

a: ESTIMATING ATMOSPHERIC LIGHT

The atmospheric light A represents the global illumination of the scene. It is a crucial parameter for dehazing as it helps estimate the amount of haze present in the image. The atmospheric light estimation can be formulated as follows:

$$A = \arg\max_{\mathbf{p}} \left\| \frac{X(\mathbf{p})}{\|X(\mathbf{p})\|} - \mathbf{t}(\mathbf{p}) \right\|, \tag{1}$$

where $\mathbf{p}$ represents a pixel position. $X(\mathbf{p})$ is the color of a pixel in the hazy image. $\mathbf{t}(\mathbf{p})$ is the estimated transmission map at position $\mathbf{p}$. The atmospheric light is selected as the color of a pixel in the hazy image with the maximum distance from the estimated transmission map value at that position.

b: ESTIMATING TRANSMISSION MAP

The transmission map $\mathbf{t}$ indicates the proportion of haze in the scene. A higher value in the transmission map corresponds to clearer regions in the image with less haze, while lower values indicate regions with more haze. The transmission map estimation can be obtained by solving the following optimization problem:

$$\mathbf{t} = \arg\min_{\mathbf{t}} \left\| \frac{X - A}{\mathbf{t}} - J \right\|^2 + \lambda \|\nabla \mathbf{t}\|^2, \tag{2}$$

where J is the ideal haze-free image. $\nabla \mathbf{t}$ represents the gradient of a transmission map. The first term in the optimization problem enforces the constraint that the product of transmission map and haze-free image should be close to the difference between hazy image and atmospheric light. The second term is a regularization term with weight λ that penalizes rapid changes in the transmission map, thus promoting smoothness.

c: INTERMEDIATE HAZE-FREE IMAGE

Once the atmospheric light A and transmission map $\mathbf{t}$ are estimated, the intermediate haze-free image I can be computed using the following restoration model:

$$I = \frac{X - A}{\mathbf{t}} + A, \tag{3}$$

By performing these steps in HRL, the deep dehazing network can effectively estimate and remove the haze from the input image, leading to better results in subsequent layers of the network. The estimation process involves solving optimization problems and applying atmospheric scattering models, which are crucial for accurately dehazing the image.

3) CONVOLUTIONAL LAYERS WITH RELU ACTIVATION

Following HRL, the network comprises several convolutional layers with ReLU activation functions. Each convolutional layer applies a set of learnable filters to the input feature maps and introduces non-linearity through ReLU activation. The convolutional layers allow the network to learn complex relationships between the input and output, while ReLU activation prevents the vanishing gradient problem. The output feature maps of each convolutional layer are denoted as Z_i, and L represents the total number of layers in the network.

$$Z_i = \text{Conv}(Z_{i-1}) + \text{ReLU}(Z_{i-1}), \quad i = 1, 2, \ldots, L, \tag{4}$$

4) POOLING LAYERS AND SKIP CONNECTIONS

The network utilizes max-pooling to downsample the feature maps and capture hierarchical representations of the input image. Additionally, skip connections are employed to facilitate the flow of information throughout the network. These skip connections directly connect the output of certain layers to the output of deeper layers, enabling better propagation of low-level and high-level features. The skip connections are essential for preserving spatial details during the dehazing process.

5) CUSTOM LAYER 2: CUSTOM SPATIAL AND SPECTRAL CONSISTENCY LAYER

The cSSCL enforces the preservation of spatial and spectral information in the dehazed output. It ensures that the dehazed image remains visually consistent with the input image in terms of structural details and color fidelity. The layer takes the intermediate haze-free image I and the hazy input image X and generates the final dehazed output $\hat{Y}$. Note that cSSCL utilize Revised Loss (RL) function with the consistency term (see Eq. 6) to enforce spatial and spectral consistency between the input and dehazed images.

6) FINAL OUTPUT LAYER

Final layer of the network generates the dehazed output $\hat{Y}$ as:

$$\text{Output: } \hat{Y} = \text{Conv}(Z_L), \tag{5}$$

where Z_L represents the output feature maps of the last convolutional layer.

By incorporating HRL and cSSCL, the deep dehazing network can restore hazy images in a way that the restored images appear natural.

B. LOSS FUNCTION

In the proposed network, a consistency term in the loss function is added to encourage the preservation of spatial and spectral information of the images during the dehazing process. This consistency term ensures that the dehazing network maintains the original radiance of the image while removing the haze. Revised Loss (RL) function with the consistency term is as follows:

$$\text{RL} = \text{MSE Loss} + \lambda \times \text{CL}, \tag{6}$$

where MSE Loss is the mean squared error (MSE) loss as defined in Eq. 7, and CL is the consistency term that measures the difference between input hazy image and dehazed image in terms of spatial and spectral information. Parameter λ controls the importance of consistency term relative to MSE loss.

MSE loss measures the difference between generated dehazed output $\hat{Y}$ and ground truth haze-free image Y. It can be computed as:

$$\text{MSE Loss} = \frac{1}{HW}\sum_{i=1}^{H}\sum_{j=1}^{W}(\hat{Y}_{ij} - Y_{ij})^2, \tag{7}$$

where $\hat{Y}_{ij}$ and Y_{ij} represent the pixel values at position (i, j) in $\hat{Y}$ and Y, respectively.

The CL is defined as follows:

$$\text{CL} = \frac{1}{HW}\sum_{i=1}^{H}\sum_{j=1}^{W}||X_{ij} - \text{Dehaze}(X_{ij})||_1 + ||\hat{Y}_{ij} - \text{Haze}(\hat{Y}_{ij})||_1, \tag{8}$$

where $||\cdot||_1$ represents L1 norm.

Dehaze(X_{ij}) and Haze($\hat{Y}_{ij}$) represent the dehazing and hazing processes applied to the input hazy image X and the generated dehazed output $\hat{Y}$, respectively.

Overall the loss function is designed to enforce two key aspects: pixel-wise reconstruction accuracy (measured by the MSE) and spatial-spectral consistency between the input hazy image (X) and the dehazed output ($\hat{Y}$). The rationale behind using the differences between the input hazy image and the dehazed image, as well as the difference between the generated dehazed image and the hazy image, lies in the following considerations:

1) SPATIAL CONSISTENCY (FIRST TERM)

$$||X_{ij} - \text{Dehaze}(X_{ij})||_1 \tag{9}$$

This term measures the pixel-wise absolute difference between the input hazy image (X) and its dehazed version. The dehazing process aims to remove the atmospheric haze while preserving the underlying scene structure. By penalizing the differences between the original hazy image and its dehazed counterpart, the network is encouraged to retain spatial details during the dehazing operation.

2) SPECTRAL CONSISTENCY (SECOND TERM)

$$||\hat{Y}_{ij} - \text{Haze}(\hat{Y}_{ij})||_1 \tag{10}$$

This term measures the pixel-wise absolute difference between the generated dehazed output ($\hat{Y}$) and its hazy version. The hazing process is essentially the introduction of atmospheric haze to a clear image. By penalizing the differences between the generated dehazed image and its hazy version, the network is encouraged to produce dehazed images that maintain the original spectral characteristics.

The combination of these two terms in the loss function (RL) ensures a trade-off between accurately reconstructing pixel values and maintaining the spatial-spectral details of the original scene. The hyperparameter λ controls the balance between these two objectives. By adjusting λ, one can influence whether the network prioritizes pixel-wise fidelity or spatial-spectral consistency.

C. TRAINING

The deep dehazing network is trained using a large dataset of paired hazy and haze-free images. The training process aims to minimize the proposed loss function by adjusting the network's parameters using Adam optimizer, which combines the benefits of both momentum-based optimization and adaptive learning rates. Adam optimizer adjusts the learning rate for each parameter based on the past gradients, making it more effective in handling different parameter updates. The update rule for Adam is as follows:

$$\text{Update rule for Adam: } \theta_i = \theta_i - \frac{\alpha}{\sqrt{v_i} + \epsilon}\hat{m}_i, \tag{11}$$

where θ_i represents the parameters of i-th layer, α is the learning rate, and ϵ is a small constant for numerical stability. $\hat{m}_i$ is the biased first moment estimate of the gradients. v_i is the biased second raw moment estimate of the gradients.

To incorporate Adam optimizer into the training process, we modify Algorithm 2 as follows:

In training process, Adam optimizer adapts the learning rates for each parameter individually, which can lead to faster convergence and better overall performance compared to the standard SGD optimizer. The hyperparameters β_1 and β_2 control the decay rates for the first and second moment estimates, respectively. The ϵ parameter is introduced for numerical stability to prevent division by zero. The algorithm continues training until the specified number of epochs

Algorithm 2 Deep Dehazing Network Training With Adam

Input: Training dataset $\{(X_i, Y_i)\}_{i=1}^{N}$, where X_i is the hazy input and Y_i is the corresponding ground truth haze-free image
Initialize the parameters of the deep dehazing network randomly
Set the learning rate α, number of epochs E, and batch size B
Initialize first moment variables $\hat{m}_i$ and second moment variables v_i for all parameters to 0
for *epoch* $= 1$ to E **do**
  for each batch $\{(X_j, Y_j)\}_{j=1}^{B}$ in the training dataset **do**
    Compute the dehazed output $\hat{Y}_j$ using the current parameters of the network
    Compute the proposed loss between $\hat{Y}_j$ and Y_j using Eq. (6)
    Compute the gradients of the loss with respect to the network parameters
    Update the first moment estimates:
      $\hat{m}_i = \beta_1 \hat{m}_i + (1 - \beta_1)\text{gradient}_i$
    Update the second moment estimates:
      $v_i = \beta_2 v_i + (1 - \beta_2)\text{gradient}_i^2$
    Compute the bias-corrected first moment estimate:
      $\hat{m}_i = \frac{\hat{m}_i}{1-\beta_1^t}$
    Compute the bias-corrected second moment estimate:
      $v_i = \frac{v_i}{1-\beta_2^t}$
    Compute the parameter update:
      $\text{update}_i = \frac{\alpha}{\sqrt{v_i}+\epsilon}\hat{m}_i$
    Update the network parameters using Adam update rule:
      $\text{param} = \text{param} - \text{update}_i$
  end for
end for
Output: Trained deep dehazing network with optimized parameters

is reached, at which point the trained deep dehazing network is ready for inference and dehazing new hazy images.

IV. PERFORMANCE ANALYSIS

In this paper, we conducted our experiments using MATLAB 2023a software, making use of both Deep Learning Toolbox and Image Processing Toolbox. Our computational setup consisted of a high-performance system equipped with an Intel Core i9 processor, 64GB RAM, and NVIDIA GeForce RTX Studio GPU.

Extensive comparisons are performed among various state-of-the-art image dehazing methods, including PDL [17], EEDNet [28], DeHRNet [29], TSDNet [15], DehazeFormer [12], DDNet [14], CPAD-Net [31], PFBN [16], and the proposed DSSCNet with different loss functions (MSE Loss, CL, and RL). The evaluations are performed on RESIDE dataset [33] using various visual and quantitative assessments.

A. DATASET

The Realistic Single Image Dehazing (RESIDE) dataset [33] serves as a comprehensive and valuable benchmark for image dehazing research. It offers a rich collection of both synthetic and real-world hazy images, covering diverse data sources and image contents. The dataset is thoughtfully organized into five subsets, each tailored for specific training or evaluation purposes. Notably, it contains a substantial training set comprising 110,500 synthetic hazy indoor images (ITS) and 313,950 synthetic hazy outdoor images (OTS). In this paper, we opted to utilize RESIDE as the benchmark dataset due to its remarkable attributes, including its large scale, diverse content, and direct relevance to real-world dehazing scenarios.

In our experiments, we partitioned RESIDE dataset into three distinct fractions: 75% for training, 15% for validation, and 10% for testing. This data decomposition strategy ensures that the deep dehazing network is trained on a substantial portion of the dataset to learn the underlying patterns and features related to haze removal.

B. HYPERPARAMETERS OF PROPOSED DEHAZING NETWORK

Table 1 shows the various hyperparameters used for training the proposed dehazing model. The learning rate (α) is set to 0.001. The model is trained for 1500 epochs with a batch size of 32. The regularization parameter (λ) is 0.01, and the first and second moment decay rates (β_1 and β_2) are 0.9 and 0.999, respectively. The epsilon value (ϵ) is set to 1e-8 for numerical stability during optimization. These hyperparameters are chosen based upon trail-and-error experiments.

TABLE 1. Hyperparameters of Proposed Dehazing Network.

Hyperparameter	Used Value (s)
Learning Rate (α)	0.001
Number of Epochs (E)	1500
Batch Size (B)	32
Regularization Parameter (λ)	0.01
First Moment Decay Rate (β_1)	0.9
Second Moment Decay Rate (β_2)	0.999
Epsilon (ϵ)	1e-8

C. VISUAL ANALYSIS

Fig. 2 illustrates the dehazing results of different image dehazing models applied to a building hazy input image. In Fig. 2(a), the hazy image serves as the input containing dense haze. Fig. 2(b) shows the result of PDL [17], which exhibits over restoration, artificial image artifacts, and degradation in edges and textures. Similarly, Figs. 2(c) and 2(d) depict the outputs of EEDNet [28] and DeHRNet [29], respectively, both demonstrating moderate darkening, edge and texture degradation, and poor spectral and spatial information preservation. Fig. 2(e) represents the result of

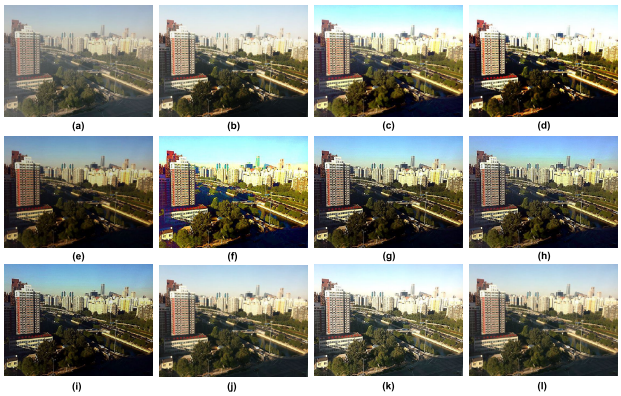

FIGURE 2. Visual analysis: (a) Building hazy image, (b) PDL [17], (c) EEDNet [28], (d) DeHRNet [29], (e) TSDNet [15], (f) DehazeFormer [12], (g) DDNet [14], (h) CPAD-Net [31], (i) PFBN [16], (j) Proposed DSSCNet with MSE Loss, (k) Proposed DSSCNet with CL, and (l) Proposed DSSCNet with RL.

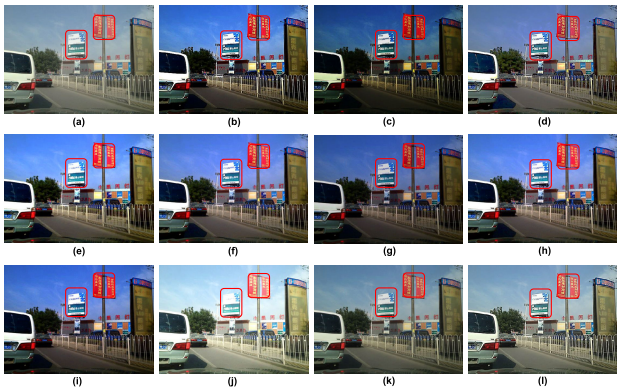

FIGURE 3. Visual analysis: (a) Road-side hazy image, (b) PDL [17], (c) EEDNet [28], (d) DeHRNet [29], (e) TSDNet [15], (f) DehazeFormer [12], (g) DDNet [14], (h) CPAD-Net [31], (i) PFBN [16], (j) Proposed DSSCNet with MSE Loss, (k) Proposed DSSCNet with CL, and (l) Proposed DSSCNet with RL.

TSDNet [15], which exhibits moderate darkening with over restoration, and similar degradation in edges and textures, along with poor spectral and spatial information preservation. Figs. 2(f) and 2(g) display the outputs of DehazeFormer [12] and DDNet [14], respectively, both showcasing over restoration, artificial image artifacts, and degradation in edges and textures, with poor spectral and spatial information preservation. In Figs. 2(h) and 2(i), the results of CPAD-Net [31] and PFBN [16] are presented, respectively. Both exhibit moderate darkening, lesser degradation in edges and textures, and moderate spectral and spatial information preservation. Finally, Figs. 2(j), 2(k), and 2(l) show the outputs of the proposed DSSCNet with MSE Loss, CL, and RL, respectively. These results demonstrate better brightness, more natural appearance, better edge, and texture preservation, as well as improved spectral and spatial information preservation compared to the other methods. The proposed DSSCNet with RL yields the most visually compelling dehazing result, showcasing its effectiveness in addressing haze removal challenges and preserving important image details.

Fig. 3 provides visual comparisons of the dehazing results obtained by different image dehazing models, with red rectangles highlighting regions of interest for better understanding. In Fig. 3(a), the road-side hazy image is the input, containing dense haze. Fig. 3(b) shows the result of PDL [17], demonstrating moderate darkening, edge, and texture degradation, along with poor spectral and spatial information preservation. Similarly, Figs. 3(c) and 3(d) depict the outputs of EEDNet [28] and DeHRNet [29], respectively, both displaying moderate darkening, edge, and texture degradation, with differing levels of spectral and spatial information preservation. Fig. 3(e) represents the result of TSDNet [15], showing moderate darkening, edge, and texture degradation, with poor spectral and spatial information preservation. Figs. 3(f) and 3(g) display the outputs of DehazeFormer [12] and DDNet [14], respectively, both showcasing moderate darkening, edge, and texture degradation, with varying levels of spectral and spatial information preservation.

In Figs. 3(h) and 3(i), the results of CPAD-Net [31] and PFBN [16] are presented, respectively, both exhibiting moderate darkening, edge, and texture degradation, along with poor spectral and spatial information preservation. Finally, Figs. 3(j), 3(k), and 3(l) show the outputs of the proposed DSSCNet with MSE Loss, CL, and RL, respectively. Overall, the proposed DSSCNet with RL yields the most promising result, providing better brightness, a natural appearance, improved edge and texture preservation, and superior spectral and spatial information, making it the most effective approach among the compared models for dehazing the input image.

D. QUANTITATIVE ANALYSIS

Table 2 provides a comprehensive quantitative analysis of various dehazing models based on three critical evaluation metrics: contrast gain (c_g), new visible edges (e), and new edge gradients ($\bar{r}$). These metrics play a crucial role in assessing the performance of dehazing algorithms in terms of enhancing image clarity, visibility of new edges, and preservation of edge gradients. The results clearly demonstrate the superiority of the proposed DSSCNet with RL, as it achieves the highest values for all three metrics.

TABLE 2. Performance comparison of different dehazing models in terms of Contrast gain (c_g), new visible edges (e), and new edge gradients ($\bar{r}$).

Model	$c_g\uparrow$	$e\uparrow$	$\bar{r}\uparrow$
PDL [17]	0.138±0.039	0.639±0.034	0.752±0.029
EEDNet [28]	0.181±0.025	0.768±0.040	0.822±0.029
DeHRNet [29]	0.182±0.025	0.684±0.044	0.860±0.023
TSDNet [15]	0.148±0.029	0.648±0.045	0.859±0.028
DehazeFormer [12]	0.142±0.022	0.630±0.022	0.691±0.025
DDNet [14]	0.119±0.023	0.762±0.033	0.714±0.032
CPAD-Net [31]	0.186±0.032	0.662±0.029	0.807±0.039
PFBN [16]	0.151±0.043	0.717±0.045	0.788±0.024
DSSCNet with RMSprop	0.174±0.021	0.725±0.031	0.826±0.019
DSSCNet with SGDM	0.176±0.022	0.758±0.029	0.810±0.024
DSSCNet with MSE	0.167±0.020	0.654±0.028	0.807±0.021
DSSCNet with CL	0.173±0.018	0.768±0.035	0.839±0.019
DSSCNet with RL	0.203±0.016	0.785±0.028	0.876±0.017

Notably, DSSCNet with RL achieves an impressive contrast gain (c_g) of 0.2003, outperforming other models such as PDL (0.138), EEDNet (0.181), and DeHRNet (0.182). This significant improvement in contrast gain highlights the effectiveness of the proposed method in enhancing image clarity and exposure, resulting in visually appealing dehazed images.

Furthermore, the proposed DSSCNet with RL excels in generating new visible edges (e) with a value of 0.7855, surpassing competing models like TSDNet (0.648), DehazeFormer (0.63), and DDNet (0.762). This higher e value signifies that the proposed model effectively reveals more visible edges in the dehazed images, leading to improved visibility and better definition of object boundaries. Additionally, the new edge gradients ($\bar{r}$) value for the proposed DSSCNet with RL is 0.8763, outperforming other models like CPAD-Net (0.807) and PFBN (0.788). The higher $\bar{r}$ value indicates that the proposed method successfully preserves edge gradients in the dehazed images, which is vital for maintaining image details and sharpness.

Table 3 provides a comprehensive performance comparison of different dehazing models based on two essential evaluation metrics: Peak Signal-to-Noise Ratio (PSNR) and Structural Similarity Index (SSIM). PSNR measures the quality of the dehazed images in terms of the signal-to-noise ratio, while SSIM assesses the structural similarity between the dehazed images and the ground truth. From Table 3, it is evident that the proposed DSSCNet with RL outperforms all other models in terms of both PSNR and SSIM. It achieves a remarkable PSNR of 29.135 and a competitive SSIM of 0.897, demonstrating the superior performance of the proposed method in generating high-fidelity dehazed images that closely resemble the original ground truth.

TABLE 3. Performance comparison of different dehazing models in terms of Peak Signal-to-Noise Ratio (PSNR) and Structural Similarity Index (SSIM).

Model	PSNR↑	SSIM↑
PDL [17]	27.195±2.837	0.892±0.040
EEDNet [28]	23.187±2.849	0.807±0.033
DeHRNet [29]	24.088±2.744	0.872±0.032
TSDNet [15]	23.473±2.884	0.852±0.032
DehazeFormer [12]	23.106±2.818	0.826±0.032
DDNet [14]	25.396±3.247	0.891±0.023
CPAD-Net [31]	24.098±2.864	0.866±0.039
PFBN [16]	24.977±3.165	0.803±0.025
DSSCNet with RMSprop	25.837±3.195	0.894±0.028
DSSCNet with SGDM	25.926±2.838	0.895±0.037
DSSCNet with MSE	24.309±2.764	0.907±0.031
DSSCNet with CL	26.528±3.084	0.888±0.043
DSSCNet with RL	29.135±2.394	0.897±0.021

E. DISCUSSION

The proposed DSSCNet with RL emerges as the superior solution for image dehazing, outperforming other models consistently across various evaluation metrics (Table 2 and Table 3). Its remarkable contrast gain (c_g) of 0.2003 enhances image clarity and exposure, crucial for applications in hazy conditions like outdoor imaging and surveillance. The model's proficiency in generating new visible edges (e) with a value of 0.7855 surpasses competing models, improving object boundary definition and aiding object detection tasks. Additionally, its ability to preserve edge gradients ($\bar{r}$) at 0.8763 ensures image details and sharpness are retained, benefiting applications like medical imaging and remote sensing.

The significant performance make the proposed DSSCNet with RL a promising solution for real-world dehazing tasks, handling dense haze, avoiding over-enhancement, and preserving texture details. In contrast, other models (e.g., PDL [17], EEDNet [28], DeHRNet [29], TSDNet [15], DehazeFormer [12], DDNet [14], CPAD-Net [31], and PFBN [16]) exhibit limitations in performance, possibly struggling with challenging hazy conditions, over-enhancement, or edge preservation.

V. CONCLUSION

In this paper, a Deep Custom Spatial and Spectral Consistency Layer-based Dehazing Network (DSSCNet) was proposed. DSSCNet's architecture incorporated custom layers, including HRL and cSSCL, to effectively estimate and remove haze from input images while preserving important spatial and spectral information. The inclusion of skip connections between layers enhanced information flow and feature extraction. The consistency term in loss function ensured that the dehazing process maintained the original content of the image, producing visually realistic and content-preserving dehazed images. The experimental results on a large dataset demonstrated the effectiveness of DSSCNet in handling various hazy conditions and producing superior dehazing results compared to existing methods. The results demonstrated that DSSCNet outperformed competitive models in terms of various performance metrics such as Contrast gain (c_g), new visible edges (e), new edge gradients ($\bar{r}$), Peak Signal-to-Noise Ratio (PSNR), and Structural Similarity Index (SSIM), exhibiting average improvements of approximately 1.27%, 1.12%, 1.18%, 1.21%, and 1.24%, respectively.

While DSSCNet has demonstrated remarkable efficacy in addressing haze removal challenges and producing high-quality dehazed images across various hazy conditions, it may encounter challenges in extreme hazy conditions or situations with unconventional atmospheric phenomena. Further investigations are needed to enhance its adaptability to such cases. Moreover, the computational requirements of DSSCNet, particularly during training, may pose constraints in resource-limited environments. Optimizing the model for efficiency without compromising its dehazing capabilities is a potential area for future research. Additionally, expanding DSSCNet to handle temporal aspects, such as video sequences, could further enhance its utility. Investigating temporal consistency and incorporating motion cues may contribute to more robust dehazing in dynamic scenes.

CONFLICT OF INTEREST

The authors declare no conflict of interest regarding the publication of this article.

ACKNOWLEDGMENT

This work was supported by the Researchers Supporting Project number (RSPD2024R968), King Saud University Riyadh, Saudi Arabia.

REFERENCES

[1] C. O. Ancuti, C. Ancuti, and C. D. Vleeschouwer, "Image dehazing guided by low-pass reinforced airlight," in *Proc. IEEE Int. Conf. Image Process. (ICIP)*, Oct. 2023, pp. 2245–2249.
[2] H. Zhou, W. Dong, Y. Liu, and J. Chen, "Breaking through the haze: An advanced non-homogeneous dehazing method based on fast Fourier convolution and ConvNeXt," in *Proc. IEEE/CVF Conf. Comput. Vis. Pattern Recognit. Workshops (CVPRW)*, Jun. 2023, pp. 1895–1904.
[3] X. Guo, Y. Yang, C. Wang, and J. Ma, "Image dehazing via enhancement, restoration, and fusion: A survey," *Inf. Fusion*, vols. 86–87, pp. 146–170, Oct. 2022.
[4] F. Erlenbusch, C. Merkt, B. de Oliveira, A. Gatter, F. Schwenker, U. Klauck, and M. Teutsch, "Thermal infrared single image dehazing and blind image quality assessment," in *Proc. IEEE/CVF Conf. Comput. Vis. Pattern Recognit. Workshops (CVPRW)*, Jun. 2023, pp. 459–469.
[5] H. Hassan, P. Mishra, M. Ahmad, A. K. Bashir, B. Huang, and B. Luo, "Effects of haze and dehazing on deep learning-based vision models," *Int. J. Speech Technol.*, vol. 52, no. 14, pp. 16334–16352, Nov. 2022.
[6] A. Fathaah, K. Ragunathan, P. Abhijith, D. R. P. M. Sekar, and P. Sankaran, "From synthetic to natural—Single natural image dehazing deep networks using synthetic dataset domain randomization," *J. Vis. Commun. Image Represent.*, vol. 89, Nov. 2022, Art. no. 103636.
[7] D. Yang and J. Sun, "A model-driven deep dehazing approach by learning deep priors," *IEEE Access*, vol. 9, pp. 108542–108556, 2021.
[8] Y. Yang, C. Hou, H. Huang, Z. Zhang, and G. Xie, "Cascaded deep residual learning network for single image dehazing," *Multimedia Syst.*, vol. 29, no. 4, pp. 2037–2048, Aug. 2023.
[9] B. Jiang, G. Chen, J. Wang, H. Ma, L. Wang, Y. Wang, and X. Chen, "Deep dehazing network for remote sensing image with non-uniform haze," *Remote Sens.*, vol. 13, no. 21, p. 4443, Nov. 2021.
[10] H. Chen, R. Chen, L. Ma, and N. Li, "Single-image dehazing via depth-guided deep retinex decomposition," *Vis. Comput.*, vol. 39, no. 11, pp. 5279–5291, Nov. 2023.
[11] C. Y. Jeong, K. Moon, and M. Kim, "An end-to-end deep learning approach for real-time single image dehazing," *J. Real-Time Image Process.*, vol. 20, no. 1, Feb. 2023.
[12] Y. Song, Z. He, H. Qian, and X. Du, "Vision transformers for single image dehazing," *IEEE Trans. Image Process.*, vol. 32, pp. 1927–1941, 2023.
[13] R. Liu, S. Li, J. Liu, L. Ma, X. Fan, and Z. Luo, "Learning Hadamard-product-propagation for image dehazing and beyond," *IEEE Trans. Circuits Syst. Video Technol.*, vol. 31, no. 4, pp. 1366–1379, Apr. 2021.
[14] Y. Li, Y. Liu, Q. Yan, and K. Zhang, "Deep dehazing network with latent ensembling architecture and adversarial learning," *IEEE Trans. Image Process.*, vol. 30, pp. 1354–1368, 2021.
[15] W. Minghu, D. Chang, W. Juan, C. Guanhai, L. Zishan, and G. Liquan, "Three subnets image dehazing method based on transfer learning," *J. Electron. Inf. Technol.*, vol. 44, pp. 3427–3434, Oct. 2022.
[16] T. Liang, Z. Li, Y. Ren, Q. Mao, and W. Zhou, "A progressive single-image dehazing network with feedback mechanism," *IEEE Access*, vol. 9, pp. 158091–158097, 2021.
[17] L. Xu and Y. Wei, "'Pyramid deep dehazing': An unsupervised single image dehazing method using deep image prior," *Opt. Laser Technol.*, vol. 148, Apr. 2022, Art. no. 107788.
[18] G. Bi, J. Ren, T. Fu, T. Nie, C. Chen, and N. Zhang, "Image dehazing based on accurate estimation of transmission in the atmospheric scattering model," *IEEE Photon. J.*, vol. 9, no. 4, pp. 1–18, Aug. 2017.
[19] J. Jackson, S. Kun, K. O. Agyekum, A. Oluwasanmi, and P. Suwansrikham, "A fast single-image dehazing algorithm based on dark channel prior and Rayleigh scattering," *IEEE Access*, vol. 8, pp. 73330–73339, 2020.
[20] T. Sharma and N. K. Verma, "Estimating depth and global atmospheric light for image dehazing using type-2 fuzzy approach," *IEEE Trans. Emerg. Topics Comput. Intell.*, vol. 6, no. 1, pp. 93–102, Feb. 2022.
[21] H. Ullah, K. Muhammad, M. Irfan, S. Anwar, M. Sajjad, A. S. Imran, and V. H. C. de Albuquerque, "Light-DehazeNet: A novel lightweight CNN architecture for single image dehazing," *IEEE Trans. Image Process.*, vol. 30, pp. 8968–8982, 2021.
[22] C. Li, J. Guo, F. Porikli, H. Fu, and Y. Pang, "A cascaded convolutional neural network for single image dehazing," *IEEE Access*, vol. 6, pp. 24877–24887, 2018.
[23] H. Zhang, V. Sindagi, and V. M. Patel, "Joint transmission map estimation and dehazing using deep networks," *IEEE Trans. Circuits Syst. Video Technol.*, vol. 30, no. 7, pp. 1975–1986, Jul. 2020.
[24] W. Wang, F. Chang, T. Ji, and X. Wu, "A fast single-image dehazing method based on a physical model and gray projection," *IEEE Access*, vol. 6, pp. 5641–5653, 2018.
[25] S. Hong, M. Kim, H. Lee, and M. G. Kang, "Nighttime single image dehazing based on the structural patch decomposition," *IEEE Access*, vol. 9, pp. 82070–82082, 2021.
[26] M. Kim, S. Hong, H. Lee, and M. G. Kang, "Single image dehazing of road scenes using spatially adaptive atmospheric point spread function," *IEEE Access*, vol. 9, pp. 76135–76152, 2021.
[27] W. Wang, X. Yuan, X. Wu, and Y. Liu, "Fast image dehazing method based on linear transformation," *IEEE Trans. Multimedia*, vol. 19, no. 6, pp. 1142–1155, Jun. 2017.
[28] A. Kalra, A. Sequeira, A. Manjunath, S. Lal, and R. Bs, "A new deep learning architecture for dehazing of aerial remote sensing images," *Multimedia Tools Appl.*, vol. 81, no. 30, pp. 43639–43655, Dec. 2022.
[29] W. Han, H. Zhu, C. Qi, J. Li, and D. Zhang, "High-resolution representations network for single image dehazing," *Sensors*, vol. 22, no. 6, p. 2257, Mar. 2022.
[30] J. Yu, D. Liang, B. Hang, and H. Gao, "Aerial image dehazing using reinforcement learning," *Remote Sens.*, vol. 14, no. 23, p. 5998, Nov. 2022.
[31] C. Song and J. Liu, "A single image dehazing method based on end-to-end CPAD-net network in deep learning environment," *J. Circuits, Syst. Comput.*, vol. 32, no. 16, Nov. 2023, Art. no. 2350272.
[32] A. S. Parihar and S. Gupta, "Dehazing optically haze images with AlexNet-FNN," *J. Opt.*, vol. 53, no. 1, pp. 294–303, Feb. 2024.
[33] B. Li, W. Ren, D. Fu, D. Tao, D. Feng, W. Zeng, and Z. Wang, "Benchmarking single-image dehazing and beyond," *IEEE Trans. Image Process.*, vol. 28, no. 1, pp. 492–505, Aug. 2019.